INTERNATIONAL JOURNAL FOR NUMERICAL METHODS IN FLUIDS
Int. J. Numer. Meth. Fluids 2004; **44**:737–763 (DOI: 10.1002/fld.672)

Verification and validation of impinging round jet simulations using an adaptive FEM

Dominique Pelletier*,†,‡, Éric Turgeon§ and Dominique Tremblay¶

Département de génie mécanique, École Polytechnique de Montréal, C.P. 6079, Succ. Centre-ville, Montréal, (Québec), Canada H3C 3A7

SUMMARY

This paper illustrates the use of an adaptive finite element method as a means of achieving verification of codes and simulations of impinging round jets, that is obtaining numerical predictions with controlled accuracy. Validation of these grid-independent solution is then performed by comparing predictions to measurements. We adopt the standard and accepted definitions of verification and validation (Technical Report AIAA-G-077-1998, American Institute of Aeronautics and Astronautics, 1998; Verification and Validation in Computational Science and Engineering. Hermosa Publishers: Albuquerque, NM, 1998). Mesh adaptation is used to perform the systematic and rigorous grid refinement studies required for both verification and validation in CFD. This ensures that discrepancies observed between predictions and measurements are due to deficiencies in the mathematical model of the flow. Issues in verification and validation are discussed. The paper presents an example of code verification by the method of manufactured solution. Examples of successful and unsuccessful validation for laminar and turbulent impinging jets show that agreement with experiments is achieved only with a good mathematical model of the flow physics combined with accurate numerical solution of the differential equations. The paper emphasizes good CFD practice to systematically achieve verification so that validation studies are always performed on solid grounds. Copyright © 2004 John Wiley & Sons, Ltd.

KEY WORDS: adaptivity; finite element; turbulent flow; two-equation model; verification; validation

INTRODUCTION

Impinging round jets are widely used for industrial applications. They produce very high heat transfer coefficients and provide a powerful approach for cooling, drying and heating operations. Many other areas such as jet painting and rocket launching also deal with such flows. Turbulent jets have received more attention than laminar ones since they are more frequently

*Correspondence to: Dominique Pelletier, Département de génie mécanique, École Polytechnique de Montréal, C.P. 6079, Succ. Centre-ville, Montréal, Québec H3C 3A7, Canada.
†E-mail: dominique.pelletier@polymtl.ca
‡Professor, Canada Research Chair.
§Graduate Student, now with Pratt and Whitney of Canada.
¶Graduate Student.

Received 1 September 2001
Revised 15 September 2003

Table I. Flow over a backward facing step.

Reference	Turbulence model	L/H
Kim *et al.*	experiment	7 ± 0.5
Mansour and Morel	k–ε	5.2
Pollard	k–ε	5.88
Rodi *et al.*	k–ε	5.8
Launder *et al.*	ASM	6.9
Abdelmeguid *et al.*	k–ε	6
Demirdzic *et al.*	modified k–ε	6.2
Donaldson *et al.*	RSM	6.1
Ilegbusi and Spalding	modified k–ε	7.2
Nallasamy and Chen	k–ε	5.8
Syed *et al.*	k–ε	5.8
Ilinca *et al.*	k–ε	6.2

encountered. Both will be considered here. However, the emphasis is on the hydrodynamics of the flow rather than on heat transfer aspects.

The study of impinging flows is particularly interesting because of the diversity of behaviour in the different parts of the flow: free-jet, impingement and wall-jet regions. The impingement region is of particular interest in the validation of turbulence models which are usually better suited for flows parallel to walls.

As already reported [1–4], much scatter is observed in results obtained by various authors. There are many possible causes to this scatter: numerical schemes, mathematical models, mesh, boundary conditions, wall treatment, etc. The objective of the present paper is to control the numerical precision of the solution so as to eliminate the mesh as a source of error. Once the accuracy is certified, validation and comparison of models may be performed on a more solid basis. Under such circumstances, the inaccuracies in predictions are due to turbulence modelling errors.

Such issues are of concern to a broad spectrum of fluid dynamics problems and have been observed in many other instances. In fact, accurate and reliable prediction of turbulent flows has been the subject of much research by the CFD community over the past few years. A review of the literature reveals that in many cases, for a given flow, predictions by different authors show an unacceptable amount of scatter. At times this gets even more disconcerting given that people using similar models and numerical algorithms produce vastly differing predictions. Table I presents the predicted length of the recirculation zone for turbulent flow over a backward facing step. All authors use a variant of the k–ε model with wall functions and a TEACH type solution algorithm [5]. The only exceptions are the predictions of Donaldson, who used a Reynolds Stress Model, and that of Ilinca *et al.* obtained with an adaptive finite element method. The only possible causes for the differences observed between authors are the meshes used and details of the computer implementation of the algorithm. The scatter between predictions is even worse for turbulent heat transfer predictions. Table II presents the maximum Nusselt number downstream of a sudden pipe expansion. These results were taken from Launder [3]. Hutton *et al.* collected the original data [6]. The largest predicted value is five times bigger than the lowest value. The lowest predicted value is in error by 50% while the highest prediction is in error by more than 100%. According to Launder the main source of error is

Table II. Maximum Nusselt number downstream of a sudden pipe expansion.

Author	Nu_{max}
Numerical #1	1660
Numerical #2	375
Numerical #3	1205
Numerical #4	1330
Numerical #5	915
Numerical #6	2036
Numerical #7	574
Numerical #8	1440
Numerical #9	921
Numerical #10	943
Numerical #11	975
Experimental	932

the near wall model. However, mesh size and artificial diffusion due to upwind discretization of convective terms provide an uncontrolled and often non-negligible source of error.

While turbulence modelling issues are still a topic of hot debate, numerical and discretization issues can now be addressed in a rigorous and systematic manner so as to minimize their impact on the uncertainty of predictions. Adaptive methods are a powerful tool to control numerical errors. It is now possible to obtain 'numerically exact' solutions to the differential equations so that mathematical modelling issues can be studied and evaluated with confidence.

Roache proposes a two-step approach in order to distinguish mathematical modelling errors and numerical errors [7]. The first step is called *verification*. Simply stated, it provides an answer to the question: *Are we solving the equations right*? Questions of numerical accuracy are at the heart of the verification process. The second step is called *validation* and provides answers to the question: *Are we solving the right equations for this problem*? The key question in validation is one of *the suitability of the mathematical model to accurately represent the physical process of interest*.

This paper proposes an adaptive finite element method as an efficient tool for performing both verification and validation. This methodology has already proved its ability to produce high quality and very accurate solutions to a wide variety of problems. Initial efforts were focused on laminar isothermal flows [8, 9], turbulent incompressible flows [10–12], and compressible flows [13]. Applications to laminar heat transfer have also been presented [14, 15], including conjugate effects [16] and compressibility [17]. Applications to turbulent heat transfer may be found in References [18–20]. Using the adaptive methodology, the paper presents examples of code verification by the method of manufactured solution. Examples of successful and unsuccessful validation show that agreement with experiments is achieved only with a good mathematical model of flow physics combined with accurate numerical solution of the differential equations. The paper emphasizes good CFD practice to systematically achieve verification so that validation studies are always performed on solid grounds.

Adaptive methods provide a powerful approach to handle flows with such a spectrum of behaviours within the flow field. Automatic grid point clustering in regions of rapid variation of the solution ensures accurate resolution in all parts of the flow. Mesh adaptation can yield 'numerically exact' (grid independent) solutions. The error estimator allows for quality

control of the solution. The adaptive strategy provides a simple means of quantifying the convergence of an adaptive grid refinement study. Our previous work on adaptive finite element methods has described both verification and validation computations for a variety of problems of practical interest [1, 10–12, 18].

The paper is organized as follows. The first section contains definitions of verification and validation to provide context. Then the governing equations are presented. The Navier–Stokes equations and standard k–ε model, coupled with wall functions, are used. We also present the logarithmic form used for preserving positivity of turbulence variables. The finite element formulation is also discussed. The next section briefly describes the adaptive methodology and the error estimator. Next, we present some examples of code verification using the method of manufactured solutions proposed by Roache [7]. Finally, the adaptive methodology is applied to a variety of laminar and turbulent impinging jets for which simulation verification and validation are performed. The paper ends with conclusions.

DEFINITIONS

First and foremost we must make the essential distinction between verification and validation. In a common English thesaurus, verification and validation are synonymous. However, in CFD these two words have acquired a generally accepted *technical meaning* which is provided in the *specific technical context* of CFD. The same words can have different technical meanings in different contexts. We follow accepted definitions [7, 21–23] and adopt the succinct description of *verification* as *solving the equations right*, and of *validation* as *solving the right equations*.

For Verification, the code author defines precisely what partial differential equations and boundary conditions are being solved and convincingly demonstrates that they are solved correctly (i.e. with some order of accuracy) and always consistently so that, as some measure of the mesh size tends to zero, the code produces a solution to the continuum equations. Whether or not those equations and that solution bear any relation to a physical problem of interest to the code users is the subject of validation. Thus in a meaningful but scrupulous sense, one cannot validate a 'code'. The best one can do is validate a simulation or perhaps a range of calculations for a well defined class of problems.

Another way do make the distinction between verification and validation is to speak of numerical errors versus conceptual modelling errors. An example is the assumption of incompressibility. For instance, dynamic stall of helicopter rotor blades entails compressibility effects at surprisingly low free-stream Mach number. Results from an incompressible flow code will likely not agree with experimental data. However, one cannot claim that code failed verification because it was applied to a compressible flow. In this case, the lack of agreement with data is not a code problem. It is a modelling problem: the user chose the wrong model for his flow.

Another way of distinguishing verification from validation is to follow the classical distinction between mathematics and engineering science. Verification is strictly an activity in the mathematics of numerical analysis. It answers the question *Are we doing good numerical analysis to solve the differential equations at hand*? Validation is essentially and strictly an activity in engineering science. It answers the question *Are we doing good engineering modelling for the problem of interest*?

This distinction is further enhanced by looking at the IEEE definition of code verification [24]: '*Formal proof of program correctness*'. We agree with Oberkampf's evaluation of this terse definition [25]: '*Although brief, this definition brings unprecedented clarity to the meaning of the term, and it adds a new perspective to the issue. Specifically, this definition bluntly requires correctness or veracity of prediction, without bringing in supportive topics as what is being predicted or how it is done*'. While more general, the IEEE definition is compatible with the one used here, and is also compatible with the distinction between Verification and Validation. That is, *program correctness* for a PDE code would naturally include *solving the equations right*, and of course a definition of what those continuum equations are, without getting into the question of whether certain problems are appropriate for those equations and that code, i.e. Validation. In other words Verification and Validation are separate steps.

Questions of numerical accuracy are at the heart of the Verification process. Thus, both the code and individual simulations must be verified. Verification of a code involves error estimation from a known solution, whereas verification of a specific calculation involves error estimation or banding to ensure that problem specification does not prevent the code from delivering the expected accuracy [7]. See Roache for cases where a verified code may deliver non-verified simulations [7].

The key question in validation is centered on *the suitability of the mathematical model to accurately represent the physical process of interest*. Predictions are compared to experiments to determine the degree of accuracy to which the model represents reality. Again, this is matter of physics and engineering, not of mathematics. Note that any validation exercise looses its significance and credibility if prior verifications (of the code and the calculations) are not performed. The rule is: verify first, validate next. Unfortunately, violations to this rule are frequently encountered in the literature. Roache recommends systematic grid refinement studies for structured non-adaptive meshes combined with Richardson extrapolation as a means of performing verification studies. In this paper, adaptive remeshing is shown to be a cost-effective alternative that automates the tedious process of manual generation of finer meshes.

To many people, Validation simply consists in comparing predictions to experimental measurements. In practice, Validation is a more difficult exercise than one would expect. One must start with *good* CFD (verified) predictions and compare them to *good* experimental data. The first difficulty to overcome is best described by the following saying in the aerodynamics community: '*No one believes the CFD prediction except the one who performed the calculation, and every one believes the experimental data except the one who performed the experiment*'. Second, good data is difficult to obtain due to experimental errors. For instance wind tunnels suffer from flow angularity and blockage effects which are further complicated because they vary with angle of attack. Furthermore, experimental data must be interpreted with care because of the possible sources of errors: calibration errors, data acquisition errors, data reduction errors, test technique errors etc. [26].

Most experiments were never designed for CFD validation. As a result some data critical to CFD is often missing: geometry, boundary conditions, initial conditions etc. [7]. Aeschliman *et al.* also report that '*as one progresses down the list to more difficult quantities for CFD to predict, the experimental uncertainty generally increases also*'. This can result in false invalidation (failed validation) or false validation. Wilcox [27] describes a case where the data were incomplete and lead to a false invalidation. Aeschliman *et al.* describe a case for

which both the CFD and experiments contained serious errors, yet agreed extremely well with each other!

The flow models and the experimental data presented in the paper were selected to illustrate a range of situations. All involve verified computations. Examples show that a verified code may lead to successful validation for one flow and failed validation for another. This highlight the delicate and difficult nature of verification and validation.

MODELLING OF THE PROBLEM

Flow equations

For laminar flow problems we use the Navier–Stokes equations for an incompressible fluid:

$$\rho u \cdot \nabla u = -\nabla p + \nabla \cdot [\mu(\nabla u + (\nabla u)^{\mathrm{T}})] \tag{1}$$

$$\nabla \cdot u = 0 \tag{2}$$

where ρ is the density, u is the velocity, p is the pressure and μ is the viscosity.

Incompressible turbulent flows are modelled by the time-averaged momentum and continuity equations.

$$\rho \boldsymbol{u} \cdot \nabla \boldsymbol{u} = -\nabla p + \boldsymbol{f} + \nabla \cdot [(\mu + \mu_t)(\nabla \boldsymbol{u} + (\nabla \boldsymbol{u})^{\mathrm{T}})] \tag{3}$$

$$\nabla \cdot \boldsymbol{u} = 0 \tag{4}$$

where ρ is the density, $\boldsymbol{u}$ is the velocity, p is the pressure, μ is the viscosity, μ_t the eddy viscosity and $\boldsymbol{f}$ is a body force. The eddy viscosity μ_{T} is computed using the standard k–ε turbulence model.

The standard k–ε model of turbulence

The eddy viscosity is expressed in terms of two turbulence variables, the turbulence kinetic energy k and its rate of dissipation ε:

$$\mu_t = \rho C_\mu \frac{k^2}{\varepsilon}$$

The mathematical system is closed by using the standard k–ε model of turbulence [28]. The transport equations for k and ε are written in a block-triangular form [10]:

$$\rho \boldsymbol{u} \cdot \nabla k = \nabla \cdot \left[\left(\mu + \frac{\mu_t}{\sigma_k} \right) \nabla k \right] + \mu_t P(\boldsymbol{u}) - \rho^2 C_\mu \frac{k^2}{\mu_t} + q_k$$

and

$$\rho \boldsymbol{u} \cdot \nabla \varepsilon = \nabla \cdot \left[\left(\mu + \frac{\mu_t}{\sigma_\varepsilon} \right) \nabla \varepsilon \right] + \rho C_1 C_\mu k P(\boldsymbol{u}) - C_2 \rho \frac{\varepsilon^2}{k} + q_\varepsilon$$

Table III. Constants for the k–ε model.

C_μ	C_1	C_2	σ_k	σ_ε
0.09	1.44	1.92	1.0	1.3

where the production of turbulence P is defined as

$$P = \nabla \boldsymbol{u} : (\nabla \boldsymbol{u} + (\nabla \boldsymbol{u})^{\mathrm{T}})$$

The constants C_1, C_2, C_μ, σ_k, and σ_ε are set to the values recommended by Launder and Spalding [28] and are given in Table III. Finally, q_k and q_ε are artificial source terms used for code verification.

Logarithmic form of the turbulence equations

While mathematically correct, the turbulence equations may cause numerical difficulties. For example, the eddy viscosity may become negative if ε becomes negative. Catastrophic breakdown of the solver usually follows such an event. In order to prevent this from happening, the logarithmic form of these equations [29, 30] is used. This amounts to the following simple change of dependent variables:

$$\mathscr{K} = \ln(k) \quad \text{and} \quad \mathscr{E} = \ln(\varepsilon)$$

which leaves the turbulence model unchanged.

The transport equations for the logarithmic variables become:

$$\rho \boldsymbol{u} \cdot \nabla \mathscr{K} = \nabla \cdot \left[\left(\mu + \frac{\mu_t}{\sigma_k} \right) \nabla \mathscr{K} \right] + \left(\mu + \frac{\mu_t}{\sigma_k} \right) \nabla \mathscr{K} \cdot \nabla \mathscr{K} + \mu_t \mathrm{e}^{-\mathscr{K}} P - \rho^2 C_\mu \frac{\mathrm{e}^{\mathscr{K}}}{\mu_t} + q_{\mathscr{K}} \quad (5)$$

$$\rho \boldsymbol{u} \cdot \nabla \mathscr{E} = \nabla \cdot \left[\left(\mu + \frac{\mu_t}{\sigma_\varepsilon} \right) \nabla \mathscr{E} \right] + \left(\mu + \frac{\mu_t}{\sigma_\varepsilon} \right) \nabla \mathscr{E} \cdot \nabla \mathscr{E} + \rho C_1 C_\mu \mathrm{e}^{\mathscr{K} - \mathscr{E}} P - C_2 \rho \mathrm{e}^{\mathscr{E} - \mathscr{K}} + q_{\mathscr{E}} \quad (6)$$

Note that the equations for logarithmic variables are equivalent to the original equations of the turbulence model. Only the computational variables are different. Hence, the turbulence model is unchanged. The eddy viscosity is now computed in the following manner:

$$\mu_t = \rho C_\mu \mathrm{e}^{2\mathscr{K} - \mathscr{E}}$$

The TKE and its dissipation are recovered by taking the exponential of computational variables. Hence, k, ε and μ_{T} remain positive throughout the domain and during the course of the iterations.

This procedure offers additional advantages. Logarithmic variables usually vary more slowly than k and ε and the ratio of the extreme values is smaller. This makes it possible to obtain solutions on very coarse meshes. The accuracy of the prediction of μ_{T} is greatly improved

so that the flow field prediction is also more accurate. Finally, improved solution accuracy is also obtained in regions of low turbulence. See Ilinca *et al.* [11] for details.

Wall boundary conditions

The standard k–ε turbulence model is not valid when the turbulent Reynolds number is low. The near-wall region is such an instance. The strategy adopted here uses wall functions which describe the solution near the wall. We use the same wall functions described in a previous paper [18]. They involve two velocity scales, u_τ (the friction velocity) and u_* (a velocity scale based on the TKE):

$$u_* = C_\mu^{1/4} k_{\mathrm{w}}^{1/2}$$

where the subscript w stands for wall value (in fact, the value at the boundary of the numerical domain). The dimensionless distance to the wall y^+ and tangential velocity u^+ are given by

$$y^+ = \frac{\rho y u_*}{\mu}$$

$$u^+ = \frac{u}{u_\tau}$$

where y is the distance normal to the wall and u is the tangential velocity. The universal velocity profile is given by

$$u^+ = y^+ \qquad \text{for } y^+ < y_c^+$$

$$u^+ = \frac{1}{\kappa} \ln(E y^+) \quad \text{for } y^+ \geqslant y_c^+$$

where κ is the Karman constant and E a roughness parameter. For smooth walls we take $\kappa = 0.42$ and $E = 9.0$. The corresponding boundary conditions for k, ε and the momentum equations, applied at a distance d to the wall, are:

$$\frac{\partial k}{\partial n} = 0$$

$$\varepsilon_w = \frac{u_*^3}{\kappa d}$$

$$\tau_w = \rho u_\tau u_*$$

$$u_{\mathrm{normal}} = 0$$

Finite element solver

The Navier–Stokes equations are solved by a Galerkin-type a finite element method [11, 12]. The equations are multiplied by a test function and integrated over the domain. Integration by parts of diffusion terms and pressure gradients leads to the Galerkin variational formulation. The equations are discretized using the Crouzeix–Raviart seven-node triangular element [31].

It uses an enriched quadratic velocity field and a linear discontinuous pressure. A quadratic interpolant is used for turbulence variables. Details are provided in Reference [10]. For highly convective flows, as in the case of turbulent flows, stabilized or upwind discretization of, Upwind, SUPG or GLS type are used. See References [16, 19] for details. For laminar flows a fully coupled formulation of the momentum and continuity equations is adopted. For turbulent flows the numerical solution algorithm proceeds in the following partly segregated manner. The Navier–Stokes and continuity equations are solved for a given field of μ_T. The $\mathscr{K}$ and $\mathscr{E}$ equations are then solved sequentially. Sub-iterations on the turbulence equations accelerate the overall convergence of the process. This loop is repeated until convergence is achieved.

ADAPTIVE METHODOLOGY

The mesh plays a key role in the accuracy of numerical predictions. It must be fine in regions of rapid variation of the solution. When used with care, adaptive methods can be a useful tool to obtain grid independent or 'numerically exact' solutions. Obviously they cannot be used as black boxes.

The present work uses the local least-squares projection error estimator described by Zienkiewicz and Zhu [32, 33]. Details of the method may be found in References [10, 29, 34]. An important issue in the present study is the fact that several dependent variables contribute to the error in the solution. To account for multiple sources of error, an error estimate is computed for each dependent variable: velocity, pressure, turbulence variables, and the eddy viscosity. Estimating the error in the eddy viscosity turns out to be critical for two reasons. First, smooth fields of k and ε can result in sharp fronts in the eddy viscosity. Second, the eddy viscosity is the only mechanism in two-equation models for transfer of momentum and turbulence by turbulent fluctuations.

The error estimates provide the information required to generate a new and improved mesh. The principle of equidistribution of the error is combined to the asymptotic rate of convergence of the finite element method to determine the element size distribution for the improved mesh. Such a formula is called a transition operator. We use the operator formulated by Hétu [10, 11, 35]. The strategy attempts to reduce the global norm of the error by a factor ξ between each adaptive cycle. Note that the transition operator is applied to each dependent variable separately to derive the appropriate mesh size for each variable including the eddy viscosity. The minimum mesh size is retained to generate the new mesh. This approach guarantees accuracy improvements for all variables.

VERIFICATION

This section presents examples of verification of the code implementing the above described adaptive finite element method. We use the method of manufactured solutions proposed by Roache [7]. The availability of an exact solution provides a rigorous framework to assess the performance and accuracy of both the flow solver and the adaptive methodology.

The first example problem considered mimics an incompressible laminar round jet impinging on a flat plate. Figure 1 illustrates the geometry for this problem. The curved boundary

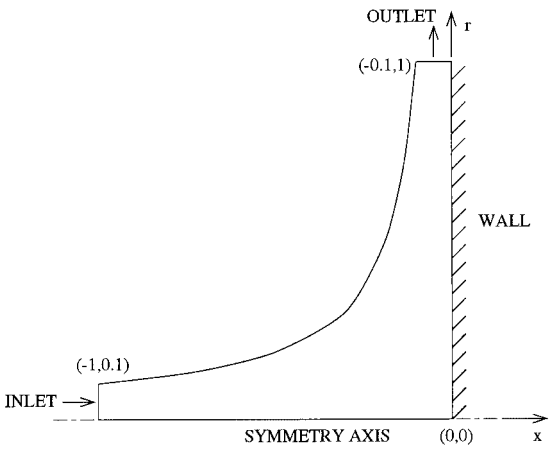

Figure 1. Geometry for the analytical jet.

correspond to a streamline where the velocity vanishes. The exact solution is given by

$$u = 100x^2(\mathrm{e}^{-x^2r^2} - \mathrm{e}^{-0.01})$$

$$v = -100xr(\mathrm{e}^{-x^2r^2} - \mathrm{e}^{-0.01})$$

$$p = \frac{1}{1 + 1000(r^2 + x^2)}$$

These expressions are substituted into the Navier–Stokes equations to determine the appropriate source term $\boldsymbol{f}$ in the momentum equations. Essential boundary conditions are applied everywhere and we set $Re = 50$.

The adaptive strategy was set to reduce the error by a factor 2 between each cycle. Ten cycles of mesh adaptation were performed. Figure 2 shows the initial very coarse mesh and the mesh obtained after seven cycles of adaptation (4726 nodes and 2257 elements). The final mesh is not shown. It has so many nodes and elements that it results in a nearly solid black image that provides no useful information. The initial mesh is very coarse and contains only one element in the cross-section of the flow. Note the mesh refinement in the stagnation point area and along the solid wall on the right hand side of the figure.

Figure 3 shows the evolution of the velocity and pressure errors during the mesh refinement process. As can be seen, the true error and its estimate decrease at each adaptive cycle indicating that the numerical predictions converge to the true solution. Furthermore, as can be seen, the error estimates get closer to the true error indicating that the error estimates converges to the true error. The error estimator exhibits asymptotic exactness. Figure 3 also plots the evolution of the efficiency indices for both velocity and pressure. The efficiency index is defined as the ratio of the estimator to the true error. As can be seen both indices converge to one with mesh adaptation, thus confirming the asymptotic exactness of the error estimators. Finally, the rate at which the errors decrease is in agreement with *a priori* estimates of the

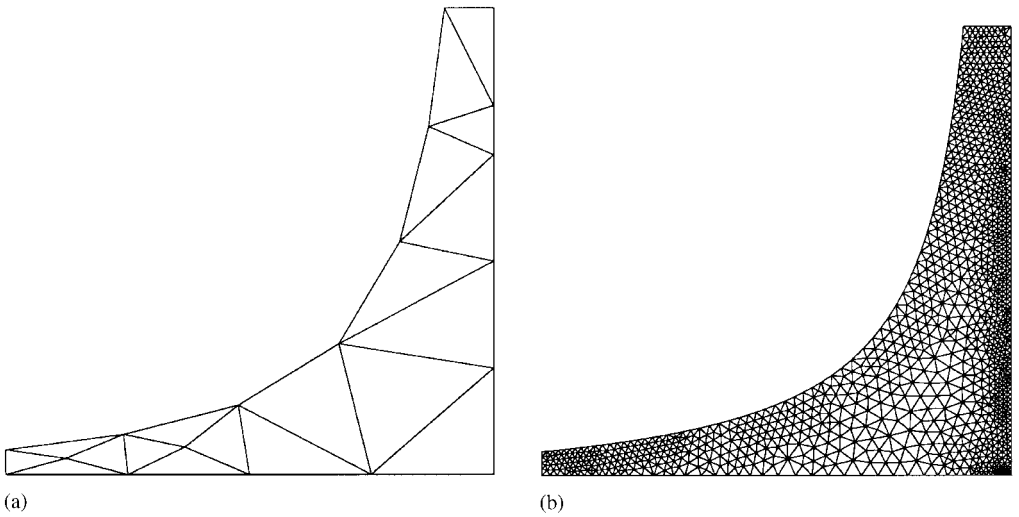

Figure 2. Meshes for the confined jet: (a) initial mesh and (b) final mesh.

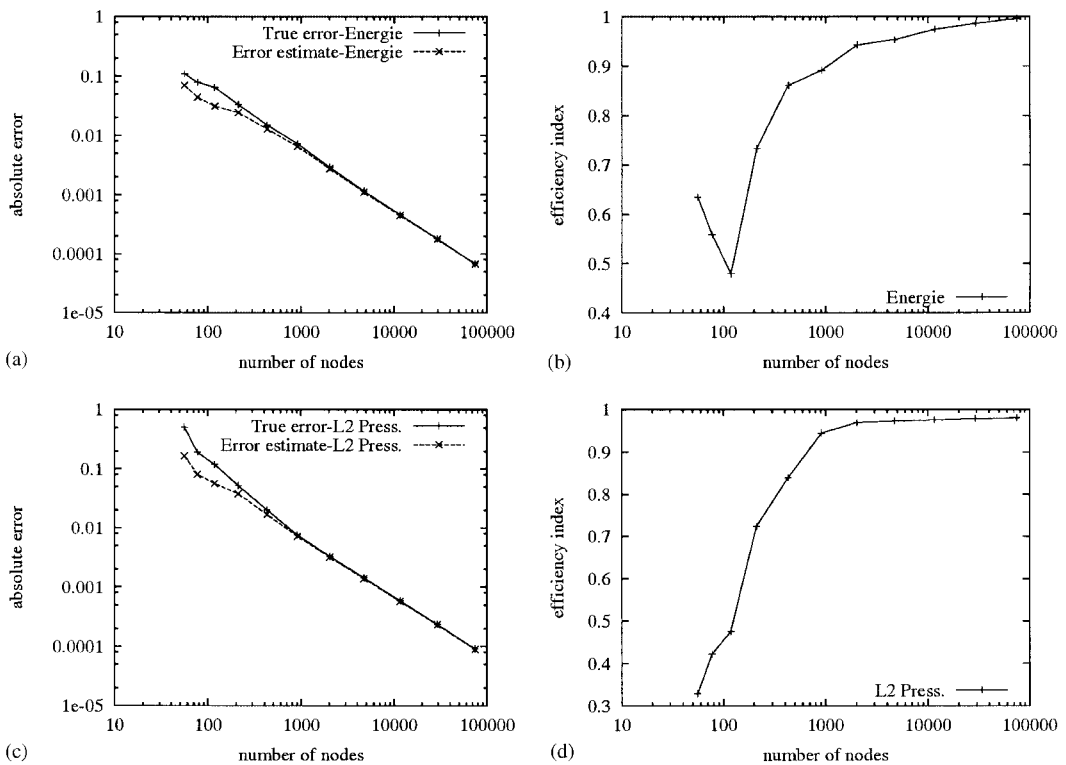

Figure 3. Convergence for manufactured laminar jet: (a) velocity error, (b) efficiency index for velocity, (c) pressure error and (d) efficiency index for pressure.

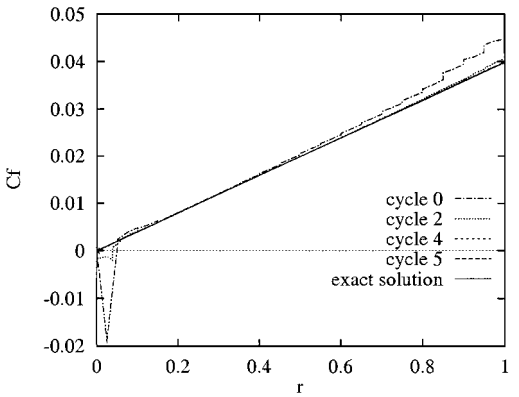

Figure 4. Skin friction coefficient distribution for the analytical jet.

convergence rates. The code is thus *verified* in the sense of Roache [7] for the flow model used in this case.

Figure 4 provides another visual representation of global convergence and high accuracy. The distribution of the skin friction coefficient along the plate is plotted ($C_f = \tau_w/(0.5\rho U^2) = (-2/Re)\partial v/\partial x$). Here again we can see that the numerical solution converges to the exact solution as the mesh is refined. Grid independence is achieved. Note that this problem is not especially demanding from a numerical standpoint.

Similar verifications were carried out for the Upwind, SUPG and GLS finite element formulations. Similar convergence behaviours were observed. Hence, these results are not reported.

The second example of code verification is taken from Turgeon's thesis and mimics a free turbulent round jet [34]. The manufactured solution is taken to be:

$$u = \frac{3}{8\pi}\frac{c}{\varepsilon_{0x}}\frac{1}{(1+(1/4)\eta^2)^2}$$

$$v = \frac{1}{4}\sqrt{\frac{3}{\pi}}\frac{\sqrt{c}}{x}\frac{\eta-(1/4)\eta^3}{(1+(1/4)\eta^2)^2}$$

$$k = 4\times 10^{-3}\frac{\mathrm{e}^{-\eta^3/5}}{x^2} + 10^{-4}$$

$$\mu_{\mathrm{T}} = 5\times 10^{-4}\mathrm{e}^{-\eta^3/5} + 5\times 10^{-5}$$

$$\varepsilon = \frac{\rho C_\mu k^2}{\mu_{\mathrm{T}}}$$

where

$$\eta = \frac{1}{4}\sqrt{\frac{3}{\pi}}\frac{\sqrt{c}}{\varepsilon_0}\frac{r}{x}$$

Table IV. Meshes for analytical turbulent jet [34].

Cycle	Number of nodes	Number of elements
0	348	155
1	658	311
2	1572	763
3	3693	1812
4	9141	4520

Table V. Velocity error for turbulent jet [34].

Cycle	Exact error	Error estimate	Efficiency index (%)
0	4.084×10^{-2}	4.029×10^{-2}	98.7
1	2.659×10^{-2}	2.173×10^{-2}	81.7
2	1.147×10^{-2}	9.520×10^{-3}	83.0
3	5.691×10^{-3}	5.024×10^{-3}	88.3
4	2.035×10^{-3}	1.848×10^{-3}	90.8

Table VI. Error for K for turbulent jet [34].

Cycle	Exact error	Error estimate	Efficiency index (%)
0	1.250×10^{0}	1.175×10^{0}	94.0
1	6.344×10^{-1}	7.181×10^{-1}	113.2
2	2.573×10^{-1}	2.567×10^{-1}	99.8
3	8.896×10^{-2}	8.642×10^{-2}	97.2
4	3.166×10^{-2}	3.085×10^{-2}	97.4

Table VII. Error for μ_{T} for turbulent jet [34].

Cycle	Exact error	Error estimate	Efficiency index (%)
0	1.075×10^{-4}	9.614×10^{-5}	89.4
1	4.099×10^{-5}	4.035×10^{-5}	98.4
2	1.195×10^{-5}	1.024×10^{-5}	85.7
3	4.435×10^{-6}	3.819×10^{-6}	86.1
4	1.592×10^{-6}	1.477×10^{-6}	92.8

Table IV provides information of the sequence of adaptive meshes. Tables V–VII present the trajectory of the error on typical variables. In these tables, the efficiency index is also defined as the ratio of the estimated error to the true (exact) error. Here again, the solution clearly converges to the exact solution of the differential equations and the error estimator performs well. The code is verified for turbulent flows in the sense of Roache [7].

The adaptive methodology is thus a powerful tool to verify a code. The mesh refinement studies are straight forward tasks as they are a natural component of the adaptive methodology. Finally, the process leads to highly accurate solutions.

APPLICATIONS

The adaptive methodology is now applied to laminar and turbulent impinging jets. Because the code and adaptive methodology have been rigorously verified, verification and validation of simulations for specific practical cases may be performed with confidence.

The first example involves a rather simple laminar flow. Yet it highlights some of the difficulties that arise when one uses old data that were never intended for validation purpose. While the Navier–Stokes equations are an exact model for laminar flows, the numerical prediction may not agree well with measurements due to some inherent problem with the experimental technique as is the case here.

This is followed by simulation of a round turbulent impinging jet. We have selected the k–ε model of turbulence with wall functions for several reasons. First, this model is very popular and is offered by all CFD vendors. Hence, there is a high probability that users will select it for their simulations. Second, wall functions result in very cost-effective simulations as they avoid the very fine meshes and high computational requirements of low Reynolds number turbulence models. Finally, there is renewed interest in wall functions development for complex industrial problems [36]. In fact, some of them have found their way in commercial CFD software and are often the recommended approach [37]. Thus, it appears reasonable and useful to illustrate Verification and Validation concepts on the standard k–ε model.

Laminar jet

The first application is a laminar impinging jet. The configuration corresponds to the experimental conditions of Scholtz and Trass [38]. The geometry and boundary conditions are shown in Figures 5 and 6. The Reynolds number is based on the inlet mean velocity and tube diameter. Data is available for three values of the Reynolds number: 750, 950 and 1744. The corresponding values of the distance L between the jet lips and the wall are $1d$, $2d$ and $4d$. The computational extends $20d$ from the axis in the radial direction and $3d$ upstream of the jet lips. A parabolic (fully developed) velocity profile is assumed at the inlet. A no-slip condition is applied at all solid walls. Symmetry is enforced along the jet axis, Neumann (traction free) conditions are used on the entrainment and outflow boundary segments.

Verification and validation studies are performed for three finite element formulations: standard Galerkin formulation, the streamline upwind formulation (SU or upwind) of Hughes and Brooks [39] and the SUPG formulation of Brooks and Hughes [40]. The SU (upwind) formulation applies the upwind test function to the convective term only while the SUPG applies it to all terms in the differential equations.

The above adaptive methodology was applied to the three jet cases. Results are presented in turn for the three values of the Reynolds number.

Typical initial and final meshes for the first jet case ($Re = 750$, $L/d = 1$) are shown in Figure 7. Obviously, each variational formulation will lead to slightly different meshes. The

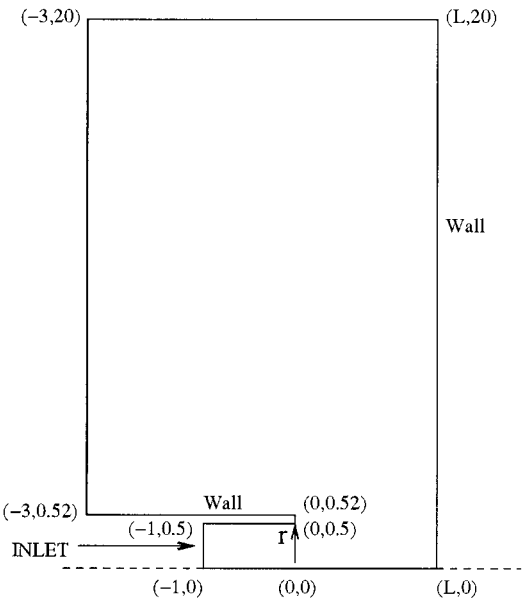

Figure 5. Geometry for the impinging laminar jet.

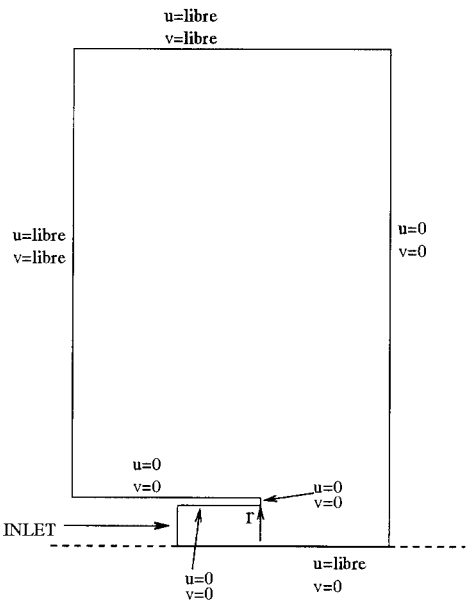

Figure 6. Boundary conditions for the laminar jet.

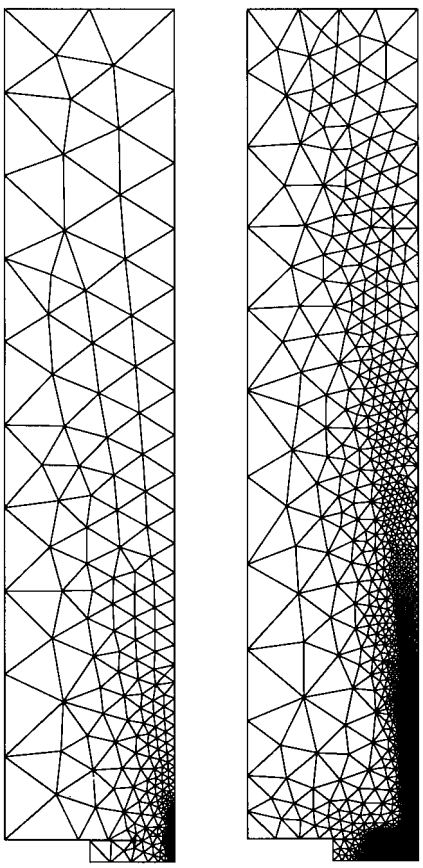

Figure 7. Initial and final meshes for $Re = 750$.

important point to note is that the same answer is obtained if one performs enough cycles of mesh adaptation.

Figure 8 presents adaptive grid convergence of the pressure coefficient along the flat plate for three variational formulations (Galerkin, SUPG and upwind). All formulations lead to grid converged results. Note however, that the Upwind formulation requires more cycles of adaptation and finer meshes than the other formulations. The important point to note is that formulations converge essentially to the same answer if the mesh is fine enough. Hence, all three simulations are verified in the sense of Roache [7].

Figure 9 compare all fine mesh predictions with the experimental data of Scholtz and Trass [38]. Agreement is excellent for the Galerkin and SUPG computation and fair to good for the Upwind simulation. The agreement is sufficiently good to claim that the three simulations are *validated* in the sense of Roache [7].

The methodology is now applied to the second jet configuration ($Re = 950$, $L/d = 2$). Typical initial and final meshes are shown in Figure 10. Results are reported for the Galerkin

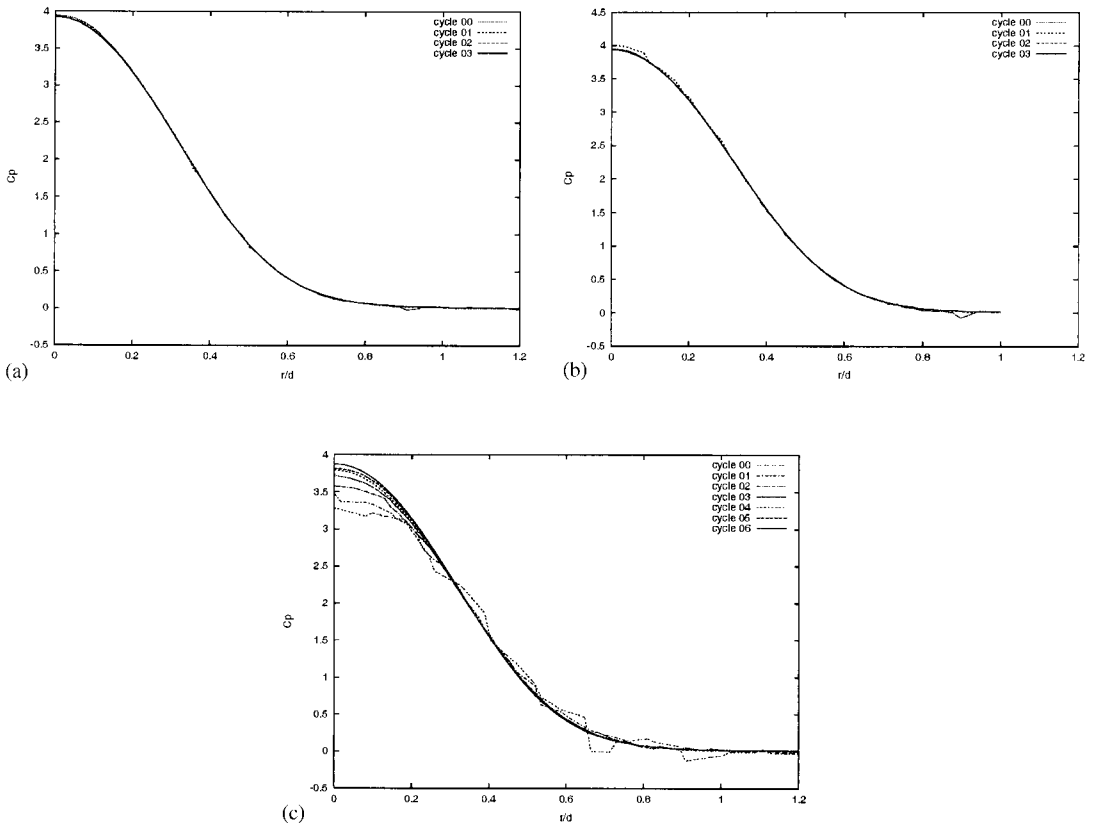

Figure 8. Grid convergence of C_p for laminar jet at $Re = 750$: (a) Galerkin, (b) SUPG and (c) upwind.

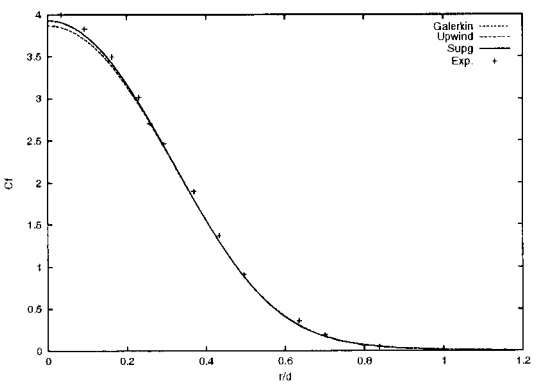

Figure 9. Validation data of C_p for laminar jet at $Re = 750$.

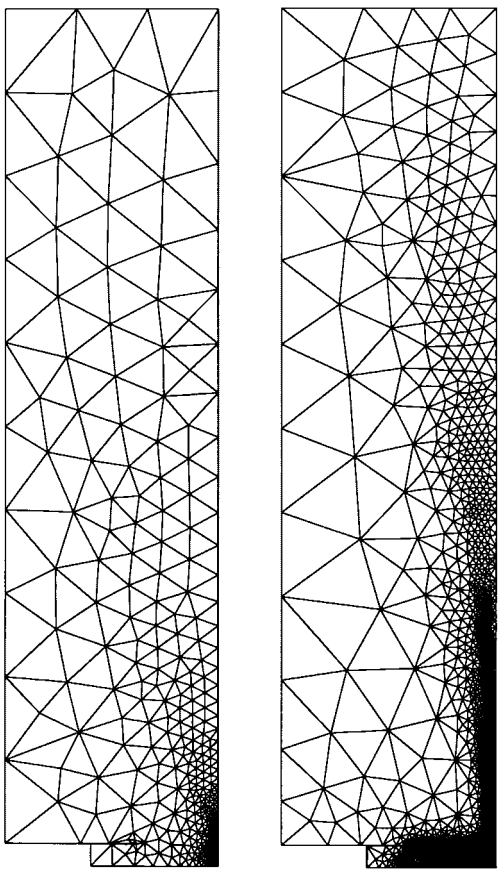

Figure 10. Initial and final meshes for $Re = 950$.

and Upwind formulation only. Convergence difficulties were encountered with the SUPG formulation.

Figure 11 presents adaptive grid convergence of the friction coefficient along the flat plate for two variational formulations (Galerkin and upwind). Both formulations lead to grid independent distributions. Hence these computations of the skin friction coefficient are *verified* in the sense of Roache [7]. Furthermore, *validation* of predictions is achieved as evidenced by the excellent agreement of grid converged predictions with the data of Deshpande and Vaishnav [41] (see Figure 12).

Finally, the methodology applied to the highest Reyolds number jet configuration ($Re = 1744$, $L/d = 4$). Typical initial and final meshes are shown in Figure 13. Results are reported for the SUPG and upwind formulation only. Convergence difficulties were again encountered with the Galerkin formulation.

Figure 14 presents adaptive grid convergence of the pressure coefficient along the flat plat for two variational formulations (SUPG and upwind). In this case, the Reynolds number is so

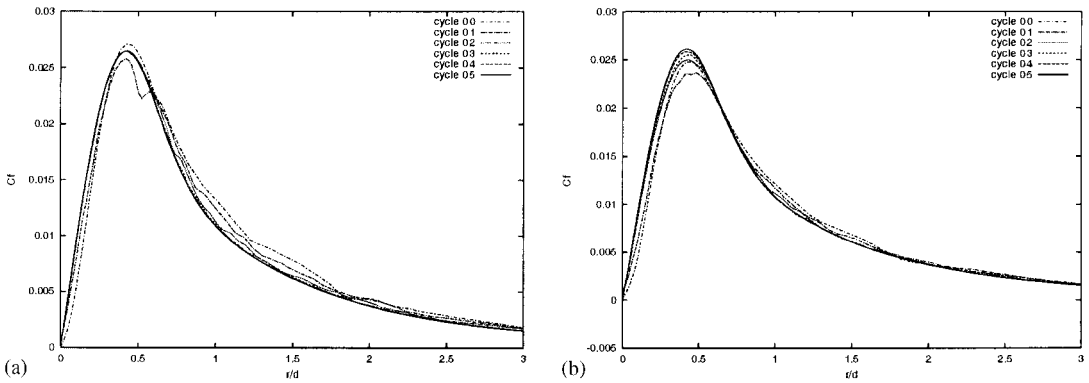

Figure 11. Grid convergence of C_f for laminar jet at $Re = 950$: (a) Galerkin and (b) upwind.

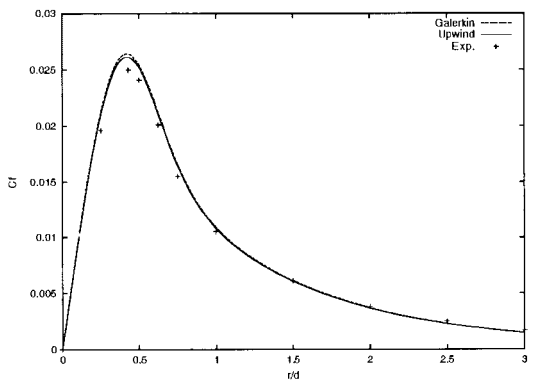

Figure 12. Validation data of C_f for laminar jet at $Re = 950$.

high that convergence of the Galerkin method could not be achieved. Both formulations lead to grid independent distributions. Hence these computations of the skin friction coefficient are also *verified* in the sense of Roache [7]. Furthermore, *validation* of predictions is achieved as evidenced by the excellent agreement of grid converged predictions with the data of Scholtz and Trass [38] (see Figure 15).

However, in all cases small discrepancies are observed between predictions and data. As explained by Roache, this is expected as the data is old and was not intended for validation purpose [7].

Turbulent jet

The second application is a turbulent round impinging jet [2]. It is an example for which the simulation, using the k–ε model with wall functions, is verified (grid convergence is observed) but not validated (predictions do not match the experiments). It has long been known that the k–ε model with wall functions is a very poor choice for this problem. We

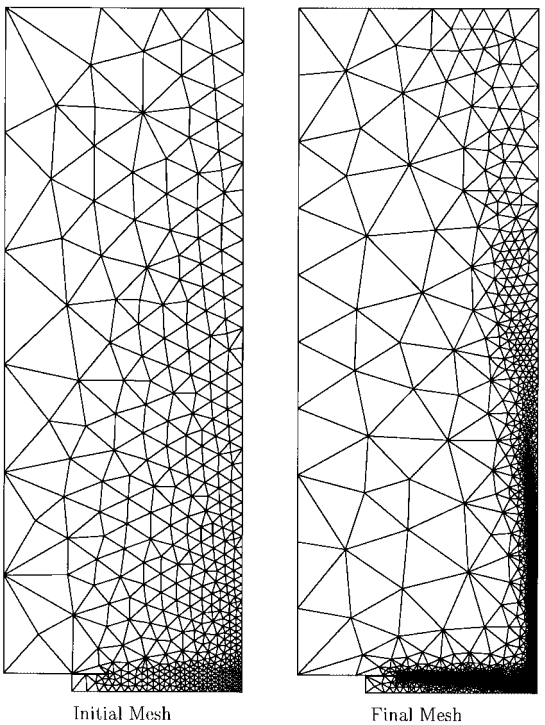

Figure 13. Initial and final meshes for $Re = 1744$.

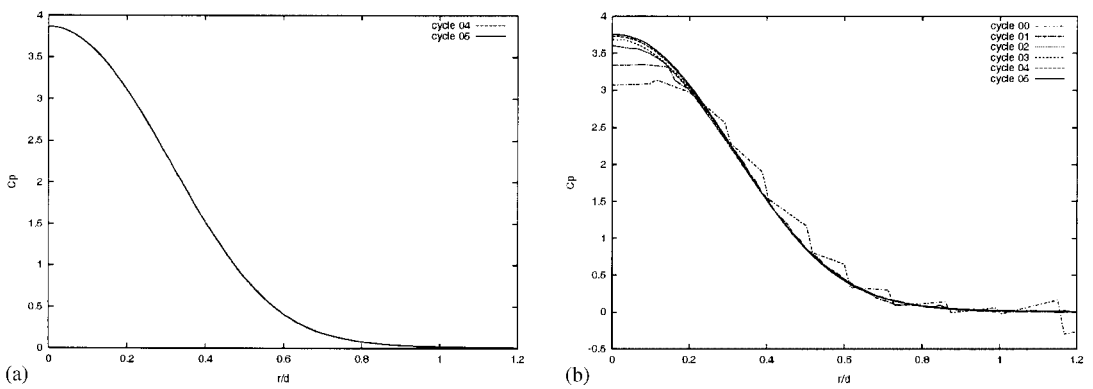

Figure 14. Grid convergence of C_p for laminar jet at $Re = 950$: (a) SUPG and (b) upwind.

still choose to include this example because it illustrates good CFD practice for producing reliable verification and validation (invalidation in this case).

The geometry is similar to that used for the laminar case. However the points $(-3, 20)$ and (2,20) of the geometry in Figure 5 are changed to $(-2, 5)$ and (2,5) to provide better grid resolution near the jet lips and the stagnation point. Initial simulations with the radial

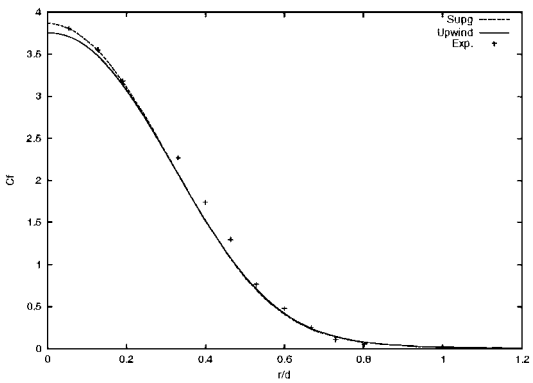

Figure 15. Validation data of C_p for laminar jet at $Re = 1744$.

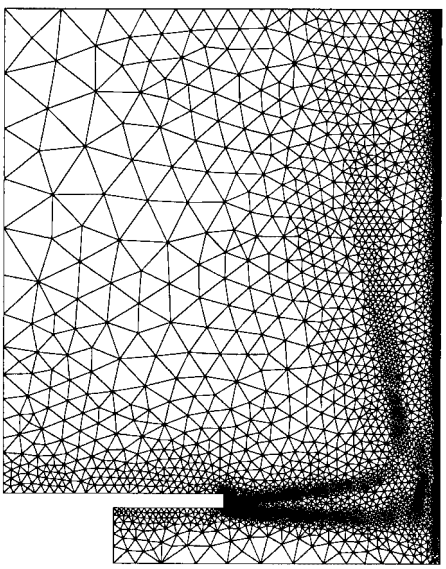

Figure 16. Final mesh for the turbulent jet.

outer boundary located at $r/d = 20$ revealed that most of the solution variations occurred within a radial distance of $r/d \leqslant 5$. The Reynolds number based on the inlet bulk velocity U and pipe diameter d is 23,000. The plate is located at a distance $L = 2d$ from the jet lips. Fully developed conditions, obtained in a separate computation, are imposed at the inlet. In this case the lip thickness is taken as $t/d = 0.132$ from the experimental configuration. The experimental data used for comparisons are those provided at the 15th Meeting of the IAHR Working Group [2].

The final mesh is shown in Figure 16. As can be seen the mesh is refined where the solution gradients are large. Notice the refinement along the wall, in the shear layer emanating for the lips, and in the regions where the jet turns into a radial wall jet.

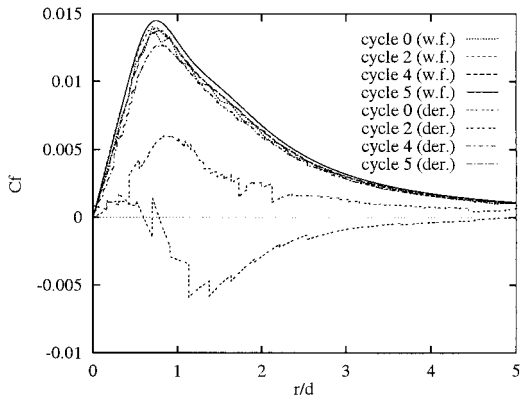

Figure 17. Skin friction distribution for the turbulent jet.

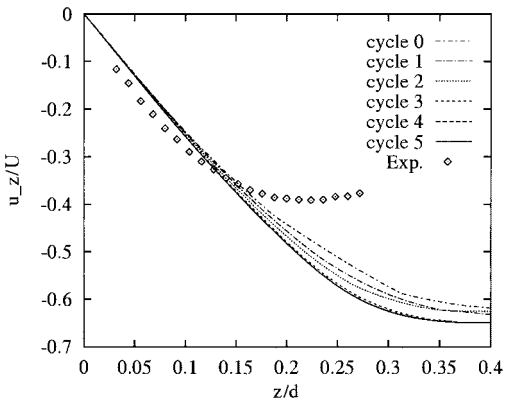

Figure 18. Turbulent jet: u_z at $r/d = 0.5$.

Figure 17 presents the distribution of the skin friction coefficient on the plate. No experimental data are available but this allows a verification of the accuracy and grid convergence of a derived quantity. Skin friction was computed in two different ways: by direct differentiation of the finite element solution ('der.' on the figure) or by using the wall functions ('w.f.') which rely only on values of v and k and not their derivatives. As can be seen, the recovery through wall functions is smoother and converges more rapidly towards its asymptotic limit. This is not surprising since it does not involve derivatives of the solution which are of lower accuracy. This fast convergence toward the exact solution of the problem modelled provides the solution to which the performance of the derivatives may be compared. The C_f computed from the derivatives is poor on the first meshes but clearly converges to the limit provided by the wall function recovery. The derivatives are not completely 'grid converged' but the benefits of adaptivity are obvious. This problem is much more demanding than its laminar counterpart. These results indicate that skin friction predictions are *verified* in the sense of Roache [7].

Figures 18–20 present distributions of u_z (the velocity in the direction z normal to the plate), v and k at $r/d = 0.5$. Similar results extracted at $r/d = 1.0$ are shown in Figures 21–23.

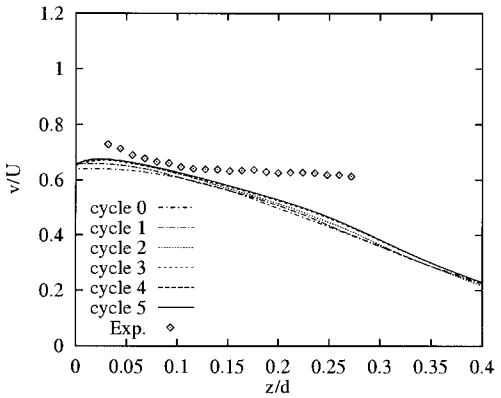

Figure 19. Turbulent jet: v at $r/d = 0.5$.

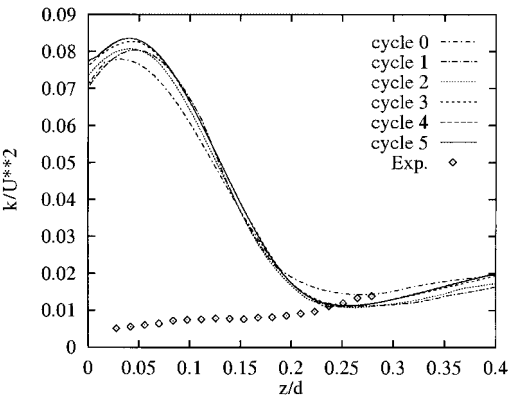

Figure 20. Turbulent jet: k at $r/d = 0.5$.

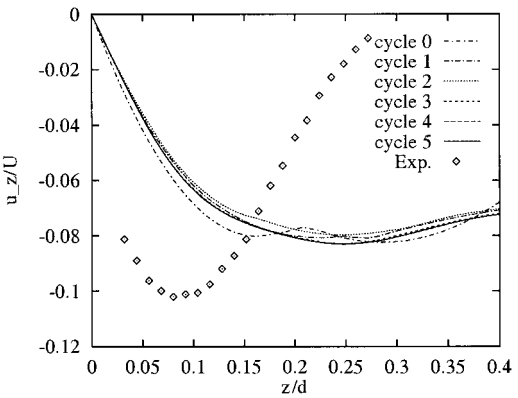

Figure 21. Turbulent jet: u_z at $r/d = 1.0$.

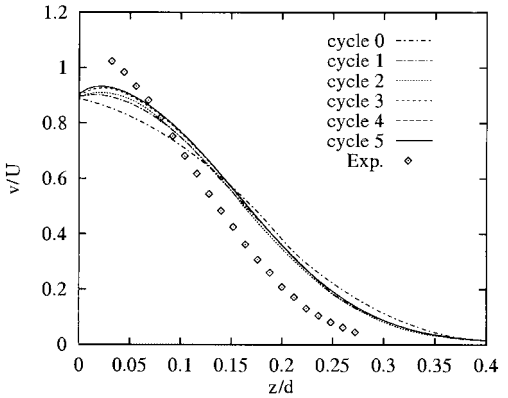

Figure 22. Turbulent jet: v at $r/d = 1.0$.

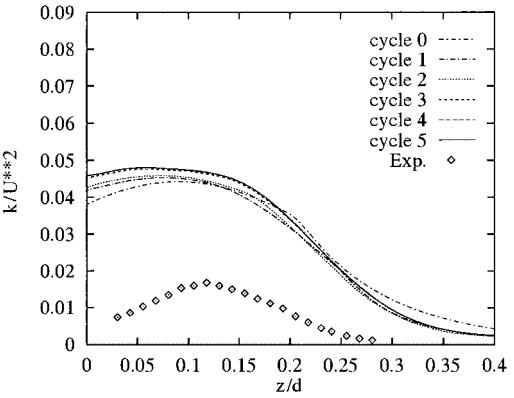

Figure 23. Turbulent jet: k at $r/d = 1.0$.

The near perfect overlay of predictions on meshes from adaptive cycles 4 and 5 indicates grid convergence of prediction and verification of the simulation in the sense of Roache [7]. Velocity predictions are at best fair, with significant discrepancies from experimental data. The predictions of the turbulent kinetic energy is nearly one order of magnitude too high! Note that the numerical solutions obtained are similar to those presented by other authors [2]. Much scatter was observed between authors. Furthermore, the k–ε turbulence model was the worst model in terms of predictive capability for k. The most important thing to observe here is the grid convergence obtained with the adaptive process. It yields grid independent solutions for all variables. The differences between predictions from meshes 4 and 5 are so small that we can conclude we have obtained the 'numerically exact solutions'. Improvements of predictions (compared to experimental data) are now a matter of turbulence modelling. However, the verification step ensures that the discrepancies are due to the mathematical model and not

the numerical scheme. Clearly, the k–ε turbulence model combined with wall functions is a poor mathematical representation of this complex flow. This striking example is presented intentionally to illustrate the differences between verification and validation and to emphasize the importance of preliminary verifications before drawing conclusions about the validity of a model. More details on this problem may be found in Reference [20].

CONCLUSIONS

An adaptive finite element methodology was shown to be a powerful tool to perform grid refinement studies. Examples reported show that the methodology can treat round incompressible laminar and turbulent jets impinging on a flat plate. With adaptivity, mesh generation is no longer a deterrent to performing grid refinement studies required for performing the rigorous verification of codes and simulations. Verification and validation become a fairly simple and straightforward process. Asymptotic exactness of the error estimators provides for quantitative estimates of the errors that are reliable enough to assess the accuracy of numerical predictions. This makes it possible to ensure that numerical errors are small enough so that verification can be performed with confidence. Examples presented show that adaptivity is no substitute for validation. It only makes the process simpler and easier to perform.

NOMENCLATURE

$C_{\varepsilon 1}$, $C_{\varepsilon 2}$, C_μ, σ_k, σ_ε	k–ε model constants
d	pipe diameter
$\boldsymbol{f}$	body force
k	turbulence kinetic energy (TKE)
$\mathscr{K}$	natural logarithm of k
L	recirculation length
p	pressure
Re	Reynolds number
$\boldsymbol{u}$	velocity
u, v	velocity components
U	reference velocity
x, r	cylindrical co-ordinates
ε	turbulence dissipation rate
$\mathscr{E}$	natural logarithm of ε
μ	viscosity
ρ	density

Subscripts

T	turbulent

ACKNOWLEDGEMENTS

This work was supported in part by the Canada Research Chair Program, the National Science and Engineering Research Council (NSERC, government of Canada) and the Fonds Québecois de la Recherche sur la Nature et la Technologie (FQRNT, government of Québec).

REFERENCES

1. Turgeon É, Pelletier D, Ignat L. Effects of adaptivity on various finite element schemes for turbulent heat transfer and flow predictions. *AIAA 36th Aerospace Sciences Meeting and Exhibit*, 12–15 January 1998/Reno, NV, AIAA Paper 98-0853.
2. Brison JF, Brun G. Round normally impinging turbulent jets. *15th Meeting of IAHR Working Group on Refined Flow Modelling*, ECL, Lyon, 1991.
3. Launder BE. Current capabilities for modelling turbulence in industrial flows. *Applied Scientific Research* 1991; **48**:247–269.
4. Cooper D, Jackson DC, Launder BE, Liao GX. Impinging jet studies for turbulence model assessment—I. Flow-field experiments. *International Journal of Heat and Mass Transfer* 1993; **36**:2675–2684.
5. Nallasamy M. Turbulence models and their applications to the predictions of internal flows. *Computers and Fluids* 1987; **15**:151–194.
6. Hutton A, Szczepura R. Turbulent flow and heat transfer in a sudden pipe expansion: a comparison of current models of turbulence. *CEGB Report TPRD/B/0926/R87*, 1987.
7. Roache P. *Verification and Validation in Computational Science and Engineering*. Hermosa Publishers: Albuquerque, NM, 1998.
8. Hétu J-F, Pelletier DH. Adaptive remeshing for viscous incompressible flows. *AIAA Journal* 1992; **30**(8): 1986–1992.
9. Hétu J-F, Pelletier DH. Fast adaptive finite element scheme for viscous incompressible flows. *AIAA Journal* 1992; **30**(11):2677–2682.
10. Ilinca F, Pelletier D. A unified approach for adaptive solutions of compressible and incompressible flows. *AIAA 35th Aerospace Sciences Meeting and Exhibit*, 6–10 January 1997/Reno, NV, AIAA Paper 97-0330.
11. Ilinca F, Pelletier D. Postivity preservation and adaptive solution for the k-epsilon model of turbulence. *AIAA 35th Aerospace Sciences Meeting and Exhibit*, 6–10 January 1997/Reno, NV, AIAA Paper 97-0205.
12. Ilinca F, Pelletier D, Garon A. An adpative finite element method for a two-equation turbulence model in wall-bounded flows. *International Journal for Numerical Methods in Fluids* 1997; **24**:101–120.
13. Ilinca F, Pelletier D, Ignat L. Adaptive finite element solution of compressible turbulent flows. *AIAA Journal* 1998; **36**(12):2187–2194.
14. Pelletier D, Hétu J-F, Ilinca F. Adaptive finite element method for thermal flows. *AIAA Journal* 1994; **32**(4):741–747.
15. Pelletier D, Ilinca F, Hétu J-F. Adaptive finite element method for convective heat transfer with variable fluid properties. *AIAA Journal of Thermophysics and Heat Transfer* Oct.–Dec. 1994; **8**(4):687–694.
16. Pelletier D, Ignat L, Ilinca F. Adaptive finite element method for conjugate heat transfer. *Numerical Heat Transfer, Part A* 1997; **32**(3):267–287.
17. Turgeon É, Pelletier D, Ilinca F. Compressible heat transfer computations by and adaptive finite element method. *37th AIAA Aerospace Sciences Meeting and Exhibit*, Reno, NV, 1999, AIAA Paper 99-0875.
18. Ignat L, Pelletier D, Ilinca F. An adaptive finite element method for turbulent heat transfer. *AIAA 34th Aerospace Sciences Meeting and Exhibit*, 15–18 January 1996/Reno, NV, AIAA Paper 96-0607.
19. Turgeon É, Pelletier D, Ignat L. Effects of adaptivity on various finite element schemes for turbulent heat transfer and flow predictions. *36th AIAA Aerospace Sciences Meeting and Exhibit*, Reno, NV, 1998, AIAA Paper 98-0853.
20. Turgeon É, Pelletier D. Computation of jet impingement heat transfer by an adaptive finite element algorithm. *7th AIAA/ASME Joint Thermophysics and Heat Transfer Conference*, Albuquerque, NM, 1998, AIAA Paper 98-2585.
21. AIAA. Guide for the verification and validation of computational fluid dynamics simulations. *Technical Report AIAA-G-077-1998*, American Institute of Aeronautics and Astronautics, June 1998.
22. Boehm BW. *Software Engineering Economics*. Prentice-Hall: Englewood Cliffs, NJ, 1981.
23. Blottner FG. Accurate Navier–Stokes results of the hypersonic flow over a spherical nosetip. *AIAA Journal of Spacecraft and Rockets* 1990; **27**(2):113–122.
24. Jay F. *IEEE Standard Dictionary of Electrical and Electronic Terms*, ANSI/IEEE Std 100, Institute of Electrical and Electronic Engineers, 1984.
25. Oberkampf WL. A proposed framework for computational fluid dynamics code calibration/validation. *18th AIAA Aerospace Ground Testing Conference*, Colorado Springs, CO, 1994, AIAA Paper 94-2540.

26. Coleman HW. Uncertainty considerations in validating CFD codes with experimental data transfer. *AIAA 27th Fluid Dynamics Conference*, New Orleans, LA, 17–20 June 1996, AIAA Paper 96-2027.
27. Wilcox D. Personal communication, 1994.
28. Launder BF, Spalding J. The numerical computation of turbulent flows. *Computer Methods in Applied Mechanics and Engineering* 1974; **3**:269–289.
29. Ilinca F. Méthodes d'éléments finis adaptatives pour les écoulements turbulents. *Ph.D. Thesis*. École Polytechnique de Montréal, 1996.
30. Ilinca F, Pelletier D. Positivity preservation and adaptive solution for the k–ε model of turbulence. *AIAA Journal* 1998; **36**(1):44–51.
31. Crouzeix M, Raviart PA. Conforming and non-conforming finite element methods for solving the stationary Stokes equations. *R.A.I.R.O.* 1973; **3**:77–104.
32. Zienkiewicz OC, Zhu JZ. The superconvergent patch recovery and *a posteriori* error estimates. Part 1: the recovery technique. *International Journal for Numerical Methods in Engineering* 1992; **33**:1331–1364.
33. Zienkiewicz OC, Zhu JZ. The superconvergent patch recovery and *a posteriori* error estimates. Part 2: error estimates and adaptivity. *International Journal for Numerical Methods in Engineering* 1992; **33**:1365–1382.
34. Turgeon É. Application d'une méthode d'éléments finis adaptative á des écoulements axisymétriques. *Master's Thesis*. École Polytechnique de Montréal, 1997.
35. Hétu J-F. Méthodes d'éléments finis adaptatives pour les écoulements visqueux incompressibles. *Ph.D. Thesis*. École Polytechnique de Montréal, 1991.
36. Grotjans H, Menter F. WAll functions for General Application CFD Codes. *ECOMAS95*, 17–20 June 1995.
37. AEA Technologies, *CFX-TascFLOW user manual*, 2001.
38. Scholtz MT, Trass O. Mass transfer in a non uniform impinging jet, Part 1 & 2. *AIChE Journal* 1970; **16**: 82–96.
39. Hughes TJR, Brooks AN. A multi-dimensional upwind scheme with no crosswind diffusion. In *Finite Element Methods for Convection Dominated Flows*, Hughes TJR (ed.), vol. 34. ASME: New York, 1979; 19–35.
40. Brooks AN, Hughes TJR. Streamline upwind/petrov–Galerkin formulations for convection dominated flows with particular emphasis on the incompressible Navier–Stokes equations. *Computer Methods in Applied Mechanics and Engineering* 1992; **32**:199–259.
41. Deshpande MD, Vaishnav RN. Submerged laminar jet impingement on a plate. *Journal of Fluid Mechanics* 1982; **114**:213–236.

